New Biological Data on a Gravettian Humerus from the Cussac Cave (Dordogne, France)

P. Guyomarc'h, V. V Sparacello, M. M Samsel, P. P Courtaud, Sébastien Villotte

BMSAP
DOI 10.3166/bmsap-2019-0063

NOTE / *NOTE*

New Biological Data on a Gravettian Humerus from the Cussac Cave (Dordogne, France)

Données biologiques inédites sur un humérus gravettien de la grotte de Cussac (Dordogne, France)

P. Guyomarc'h · V. Sparacello · M. Samsel · P. Courtaud · S. Villotte

Received: 4 March 2019; Accepted: 27 May 2019

Abstract This article reports on a complete left human humerus from the Cussac Cave (Dordogne, France), dating to the Gravettian, or Mid-Upper Palaeolithic. This humerus is characterised by a very marked retroversion, significant intracortical porosity, an unusual morphology and orientation of the medial epicondyle, and a marked depression at the bottom of the olecranon fossa. These morphological features could be related to mechanical stimuli, but this is just an assumption given the absence of control data for many factors (e.g. age-at-death, sex, body mass, degree of asymmetry). Nevertheless, the description of this new discovery contributes significantly to our understanding of the range of variation of known Late Pleistocene skeletal morphology.

Keywords Mid-upper palaeolithic · Morphometry · Biomechanics · Cross section · MicrotomographyAU: "Microct" has been changed to "Microtomography". Please confirm

Résumé Cette étude porte un humérus gauche complet issu de la grotte de Cussac (Dordogne, France), daté du Gravettien (ou Paléolithique supérieur moyen). Cet humérus est caractérisé par une rétroversion extrêmement marquée, une importante porosité intracorticale, une morphologie et une orientation particulière de l'épicondyle médial, ainsi que par la présence d'une dépression profonde au fond de la fosse olécranienne Merci de vérifier. Ces caractéristiques morphologiques pourraient être associées à des contraintes biomécaniques, mais cela reste une hypothèse en l'absence de contrôle pour de nombreux facteurs (par exemple : âge au décès, sexe, masse corporelle, degré d'asymétrie). Cette étude contribue néanmoins de façon significative à l'enrichissement de nos connaissances de l'étendue de la variation morphologique connue pour le Pléistocène récent.

Mots clés Paléolithique supérieur moyen · Morphométrie · Biomécanique · Sections transverses · Microtomographie

P. Guyomarc'h
ADES, UMR 7268, Anthropologie bioculturelle,
Droit, Éthique et Santé, CNRS, EFS,
faculté de médecine secteur nord,
Aix Marseille Université, 51, boulevard Pierre-Dramard,
F-13344 Marseille cedex 15, France

V. Sparacello · M. Samsel · P. Courtaud · S. Villotte (✉)
UMR 5199 PACEA, université de Bordeaux,
bâtiment B8, allée Geoffroy-Saint-Hilaire,
CS 50023, F-33615 Pessac cedex, France
e-mail : sebastien.villotte@u-bordeaux.fr

Introduction

While our knowledge of the palaeobiology of the Gravettian people (ca. 34–26 000 cal. BP) has grown dramatically in the last 20 years, thanks to new discoveries and new analyses of previously discovered material [e.g. 1–6], new data on skeletal remains from this period are still needed to complete our understanding, as they illustrate the morphological variability of that time. Analyses of these data not only help investigations on microevolutionary processes during the Late Pleistocene but also on past behaviour patterns and mortuary practices [6–11]. This article presents unpublished biological data on a humerus from the Cussac cave, which hosts human remains and displays art dated to the Gravettian.

The cave at Cussac, discovered in 2000, contains several hundred human remains belonging to at least five individuals, found in three different loci [12]. Analyses of the rock art and of human/animal traces have confirmed that human activities in the cave probably took place around 28–29 ky cal. BP [13]. Although only one human bone from Locus 1 has been directly dated, the two other loci are also considered as Gravettian [6,13–15].

The third locus encompasses a large area with human bones visible on an elevated platform with four depressions

and a stalagmitic pillar, and a slope with scattered human remains at different levels, including at the base (Fig. 1). A total of 106 human remains have been visually identified for the third locus, which is certainly a very conservative minimum due to the fact that observations could only be performed from the walkway [16]. The layer of clay on the slope and at its base also probably covers additional remains, and only a proper excavation (currently not possible for conservation reasons) would produce a more comprehensive understanding of the L3 formation and its taphonomic history [16].

Because of the unique character of Cussac Cave, which is listed as a Historic Monument, a non-invasive analytical methodology was applied [6,13–16]: most of the investigations are based on in situ observations and on virtual anthropology from a high-definition 3D photogrammetric record. However, exceptional authorisation was granted to temporarily extract an easily accessible and complete left adult humerus to allow more in-depth biological study of this bone (Fig. 1).

Materials and Methods

The L3-088 humerus lay in an isolated position at the base of Locus 3 (Fig. 1). Authorisation was given for it to be collected — on the condition that it would be replaced in situ after study — for taphonomic and biological analyses, as no excavation was required and no trespassing on the preserved floor was necessary (it could be reached directly from the walkway). High-definition photogrammetric records of the bone were made before and immediately after its extraction in 2014, and before its reintroduction into the cave in 2017. Additionally, micro-computed tomography (μCT) was performed in 2015. The humerus was scanned at a cubic voxel resolution of 120 μm using a GE Phoenix microtomography device at the Bordeaux PACEA/PLACAMAT microtomography platform.

Macro- and microscopic examinations, including observations of the microstructure of the cortical bone, were carried out. The completeness of the L3-088 humerus allowed both traditional [17] and additional measures employed for fossil individuals [18–20] to be taken. Data were collected twice: on the physical bone with manual sliding callipers and an osteometric board, and on the reconstructed μCT model (previously segmented manually using AVIZO v. 9 to exclude the remaining sediment attached to the bone) using TIVMI software [21], which offers multiple plug-ins to create landmarks, segments, planes, angles and outlines to ensure objective reproduction of traditional measurement protocols. Strict consistency was observed between the physical and virtual values.

Cross sections at 50% and 35% of the diaphysis were analysed in order to obtain total cross-sectional area, cortical area and variables correlating with the bending moments (second moments of area: I) and overall torsional rigidity

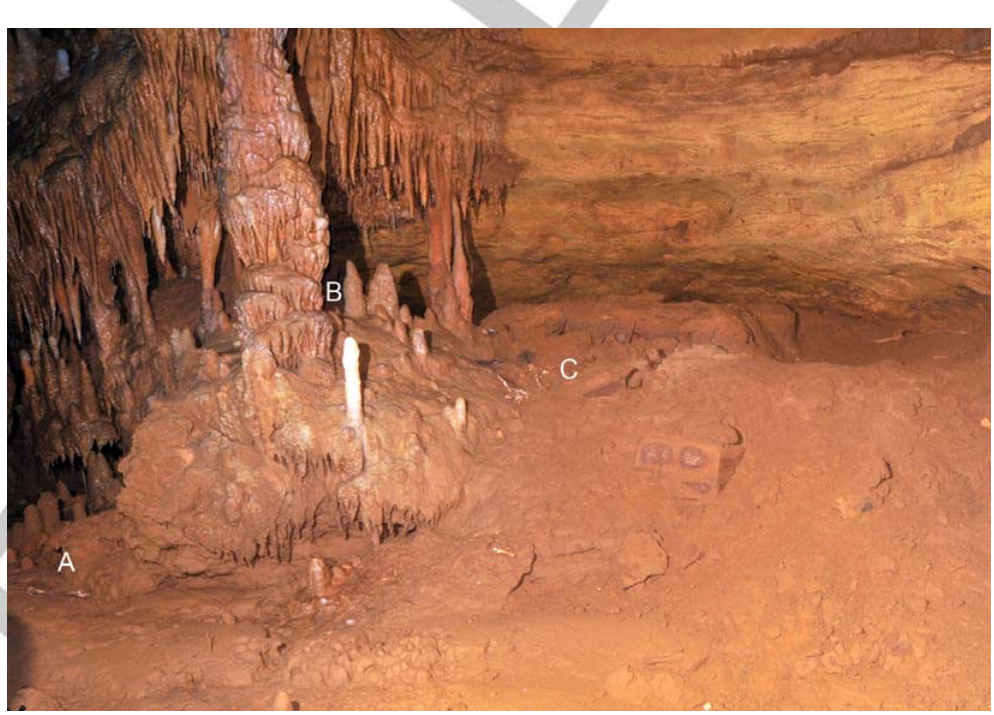

Fig. 1 General view of Locus 3. A. The isolated humerus L3-088. B. Platform. C. Slope with the main concentration of bones / *Vue générale du Locus 3. A. L'humérus isolé L3-088. B. La plateforme. C. Principale concentration d'ossements sur la pente*

(polar moment of area: J). The 3D model of the humerus was virtually positioned according to the reference planes following Ruff [22]; cross sections were obtained with Autodesk®, Netfabb® 2017 and Meshmixer 2015, v.11 and analysed with a version of the SLICE programme [23], adapted as a macro-routine inserted into NIH Image 1.52.

The data obtained were compared to humerus samples from the Mid- and Late-Upper Palaeolithic (respectively MUP and LUP). MUP individuals are mainly associated with the Gravettian, whereas LUP individuals are mainly dated to the Magdalenian and Epigravettian (recent and final) periods [see 5 for a comprehensive description of the samples]. All the individuals are adults (with a few late adolescent subjects); those presenting pathologies potentially modifying humeral morphology were excluded. The data were collected by the authors or from the literature. As humeral torsion has been described slightly differently by biological anthropologists and by clinical and sports physicians, and because data on this angle are relatively complex to collect without proper material [24], we used the data published by Rhodes and Churchill [19] for Upper Palaeolithic samples, but excluding some individuals who were not securely dated or are now directly dated to the Holocene (e.g. Veyrier 1 [25]).

To be comparable among individuals, cross-sectional properties need to be standardised by body size, usually by scaling them by bone length and by the body mass of the individual [26]. This was impossible in the case of Cussac L3-088 due to the absence of measurable elements correlated with body mass (i.e. the femoral head, or stature and bi-iliac breadth). We therefore used the humeral articular length$^{5.33}$ [27] to estimate the relative overall torsional rigidity of this bone. Standardised J was computed as standardised $J = (J/\text{Articular length}^{5.33}) \times 10^{12}$.

The stature of the individual represented by the L3-088 humerus was estimated using the Trotter and Gleser [28] equation for African-Americans, as suggested by Formicola [29] for European Mid- and Upper Palaeolithic specimens.

Results

The measurements for Cussac L3-088 are given in table 1. This left humerus is complete (Fig. 2). Most of its surface is covered by a thin brown calcite crust. There is no trace of anthropic or faunal activity, except for some small red and black stains probably related to funerary practices (i.e. use of pigments). There is some breakage of the proximal extremity with bone loss at the greater tubercle and, posteriorly, on the articular surface. Cortical bone is locally missing in the distal part of the posterior surface of the diaphysis, and the distal extremity is locally eroded.

The bone presents no major deformation in its general conformation. No degenerative or inflammatory indications involving bone were observed, and there is no trace suggestive of an in vivo fracture.

MUP humeri are significantly longer than LUP ones (Table 2) when the sample is divided by sex. The maximum length of Cussac L3-088 falls in the overlap between the known range of variation of left humeri of MUP males and females and in the upper part of the known range of variation for LUP males (Table 2). For instance, its maximum length is identical to those for the left humerus of Paglicci 25 (Italy, MUP, female) and Rochereil 1 (France, LUP, male). Based on the maximum length of the humerus, the stature of this individual is estimated at between 1.61 and 1.75 m (Table 3).

The margin of the proximal articular surface is slightly irregular but no other sign of joint alteration is visible. There is no visible entheseal change, except for a small lacuna at the attachment site of the *m. subscapularis*, but it is unclear whether this is due to taphonomic or biological processes. Cussac L3-088 displays a wide retroversion angle (low torsion) relatively to the mean obtained from the comparative samples (Table 2). Its value of 46.0° is the highest known for the left side for the Upper Palaeolithic and for the right side; it is exceeded only by two individuals, Cap-Blanc and Rochereil I.

The shaft appears laterally convex. The deltoid tuberosity has two branches, the lateral one being well developed and forming a ridge about 8 mm thick and 65 mm long, while the anterior one is very faint. Marked intracortical porosity is observed at three main locations, at the attachment sites of the *mm. deltoïdus*, *brachioradialis* and *triceps brachii* (medial head) (Fig. 3). The morphology at mid-diaphysis is roughly circular, as expressed by the values of the ratios between maximum/minimum diameter and Imax/Imin at mid-shaft, both close to 1 (respectively 1.18 and 1.19). These values are low compared to those obtained for the comparative samples (Table 2), in which a difference is seen between the MUP and LUP samples (significantly greater in MUP), sexes (usually greater in males) and sides (greater for the right side). The value for the M5/M6 ratio for Cussac L3-088 falls close to the mean for the MUP male sample for the left side. Only two individuals have lower values than Cussac L2-088 for the Imax/Imin ratio for the left humerus (Sunghir 1, an MUP male with highly asymmetrical upper limbs, and the LUP female Oberkassel 2), and none for the right humerus. With a mid-shaft circumference of 60.9 mm, close to the MUP and LUP mean values for the left side (Table 2), the Cussac humerus does not appear to be particularly distinctive. The standardised J at mid-shaft (530.4) falls close to the mean of the MUP female sample for the left side (Table 2).More distally, there is a marked anterior concavity of the Cussac L3-088 diaphysis (Fig. 2). In this region, a shallow longitudinal sulcus is visible.

Table 1 Measurements of the Cussac L3-088 humerus. All measurements are in millimetres except the cubital, torsion and retroversion angles (in degrees) and the cross-sectional properties (areas in mm^2: second moment of areas is in mm^4) / *Mesures pour l'humérus L3-088. Toutes les mesures sont en millimètres à l'exception des angles condylodiaphysaire, de torsion et de rétroversion (en degrés) et des propriétés de section (surfaces en mm^2 et seconds moments en mm^4)*

Measure	M	Reference	Cussac L3-088
Maximum length (head–trochlea)	M1	[16]	323.0
Articular length (head–capitulum)	M2	[16]	320.0
Proximal epiphysis breadth	M3	[16]	47.4
Distal epicondyle breadth	M4	[16]	62.0
Maximum diameter at mid-shaft	M5	[16]	20.6[a]
Minimum diameter at mid-shaft	M6	[16]	17.5[a]
Minimum deltoid diameter	M6a	[16]	18.3[a]
Minimum circumference of the shaft	M7	[16]	60.0
Circumference at mid-shaft	M7a	[16]	60.9[a]
Head circumference	M8	[16]	(140)
Medio-lateral head diameter	M9	[16]	(40.5)
Anteroposterior head diameter	M10	[16]	47.8
Trochlear breadth	M11	[16]	25.5
Capitular breadth	M12	[16]	16.4
Width of the articular surface (trochlea–capitulum)	M12a	[16]	46.0
Capitular height	M12c	[16]	21.6[a]
Olecranium fossa breadth	M14	[16]	29.2
Olecranium fossa depth	M15	[16]	11.0
Cubital angle (diaphysis axis vs trochlea axis)	M16	[16]	97.9[a]
Torsion angle (head axis vs trochlea axis)	M18	[16]	134.2[a]
Retroversion angle		[18]	46.0[a]
Biomechanical length (head–lateral trochlea)		[19]	317.0
Supracondylar anteroposterior diameter		[19]	16.0
Anteroposterior head arc		[19]	65.0
Medio-lateral head arc		[19]	63.6[a]
Thickness of the medial pillar		[19]	6.5
Thickness of the lateral pillar		[19]	15.2
Anteroposterior deltoid diameter		[18]	20.6[a]
Medio-lateral deltoid diameter		[18]	22.3[a]
Deltoid circumference		[18]	64.4[a]
Mid-distal (35%) total area			256.4
Mid-distal (35%) cortical area			185.6
Mid-distal (35%) Ix			5470.0
Mid-distal (35%) Iy			4343.2
Mid-distal (35%) Imax			5686.6
Mid-distal (35%) Imin			4126.6
Mid-distal (35%) J			9813.3
Standardised mid-distal (35%) J			435.9
Mid-shaft (50%) total area			284.8
Mid-shaft (50%) cortical area			203.1
Mid-shaft (50%) Ix			6105.7
Mid-shaft (50%) Iy			5834.7
Mid-shaft (50%) Imax			6483.1
Mid-shaft (50%) Imin			5457.2
Mid-shaft (50%) J			11940.3
Standardised mid-shaft (50%) J			530.4

M# indicates a measure following the Martin' system. (#) indicates estimated measurements.. Standardised J = (J/Articular length$^{5.33}$) × 10^{12} / *M# indique une mesure prise suivant le système de Martin. (#) indique une mesure estimée. Standardisation J = (J / longueur articulaire$^{5.33}$) × 10^{12}*

[a] Indicates a measurement obtained from the 3D model / *Indique une mesure obtenue à partir du modèle 3D* Merci de vérifier les notes de tableau

Fig. 2 Views of Cussac L3-088. Clockwise from top left: anterior, lateral, medial, posterior (scale = 10 cm), inferior and superior (not to scale) / *Vues du spécimen Cussac L3-088. Dans le sens des aiguilles d'une montre en partant du côté supérieur gauche : antérieure, latérale, médiale, postérieure (échelle = 10 cm), inférieure et supérieure (pas à l'échelle)*

Supracondylar ridges are only slightly marked on the anterior surface of the shaft. The robusticity index [(minimum

Table 2 Descriptive statistics for the main humeral variables for the MUP and LUP samples. The data are presented as mean ± standard deviation (number of individuals). All measurements are in millimetres except the retroversion angle (in degrees) and the indices, which are dimensionless / *Statistiques descriptives pour les principales variables humérales pour les échantillons MUP et LUP. Les données sont présentées comme moyenne ± écart-type (nombre d'individus). Toutes les mesures sont en millimètres à part l'angle de rétroversion (en degrés) et les indices qui sont sans dimensions*

		MUP			LUP		
		All indiv.	**F**	**M**	**All indiv.**	**F**	**M**
M1	Right	347.3 ± 23.7 (11)	329 ± 16.5 (4)	363.9 ± 15 (6)	304.9 ± 17.5 (20)	294.5 ± 18.2 (6)	311.8 ± 12 (11)
	Left	337.9 ± 19.1 (12)	324.5 ± 11.5 (4)	349.5 ± 19.3 (6)	302.5 ± 17.8 (18)	285.1 ± 17.1 (6)	309.9 ± 10.8 (10)
M2	Right	342.7 ± 24.4 (10)	317.5 ± 10.5 (3)	359.3 ± 14 (6)	297.7 ± 19.5 (11)	276.9 ± 24.6 (3)	305.5 ± 10.8 (8)
	Left	333.1 ± 21 (9)	305.5/318.0 (2)	344.2 ± 21.2 (5)	299.9 ± 13.1 (12)	288.8 ± 11.7 (4)	305.5 ± 10.1 (8)
M3	Right	50.6 ± 3.2 (8)	49.5 ± 1.8 (3)	52.9 ± 1.7 (4)	47.7 ± 2.8 (16)	46.1 ± 1.9 (6)	49.4 ± 2.2 (9)
	Left	50.7 ± 2.2 (5)	49.0/50.0 (2)	51.4 ± 2.6 (3)	48.2 ± 2.9 (15)	45.9 ± 0.8 (4)	49.1 ± 3.3 (9)
M4	Right	61.5 ± 3.8 (9)	59.7 ± 3.2 (3)	63.7 ± 2.7 (5)	58.9 ± 4.2 (21)	55.6 ± 3.5 (5)	60.7 ± 3.2 (12)
	Left	61.4 ± 4.9 (11)	56.0 / 62.0 (2)	63 ± 4.7 (7)	57.9 ± 4.3 (20)	52.8 ± 2.8 (6)	60.3 ± 2.7 (11)
M5	Right	23.2 ± 1.8 (13)	21.5 ± 1.6 (5)	24.4 ± 0.9 (7)	22.6 ± 2.6 (25)	20.9 ± 2.7 (8)	23.7 ± 1.7 (13)
	Left	21.4 ± 1.5 (16)	20.5 ± 1.4 (4)	21.8 ± 1.5 (10)	21.1 ± 2.5 (22)	19.3 ± 2 (8)	22.1 ± 2.5 (11)
M6	Right	18.5 ± 1.3 (13)	17.5 ± 1.4 (5)	19.3 ± 0.7 (7)	17.1 ± 2.4 (25)	16.1 ± 2.3 (8)	18 ± 2.3 (13)
	Left	17.6 ± 1.4 (16)	16.6 ± 1.7 (4)	17.9 ± 1.3 (10)	16.2 ± 2.6 (23)	15.1 ± 2.1 (8)	16.9 ± 3 (12)
M7	Right	65.2 ± 5.6 (14)	59.6 ± 4.7 (5)	68.9 ± 2.6 (8)	61.5 ± 6 (25)	57.4 ± 7.2 (8)	64.3 ± 2.6 (13)
	Left	60.7 ± 4.3 (17)	59.4 ± 6.4 (5)	61.6 ± 3.2 (10)	58.3 ± 6.6 (25)	55.1 ± 7 (10)	60.2 ± 6.1 (12)
M7a	Right	68 ± 5.8 (12)	61.6 ± 5 (4)	71.4 ± 2.7 (7)	66.3 ± 3.8 (8)	59.1 (1)	67.3 ± 2.7 (7)
	Left	63.8 ± 5.3 (16)	60.9 ± 6.1 (4)	64.7 ± 4.6 (10)	61.8 ± 5.9 (10)	59.2 ± 3 (3)	62.9 ± 6.7 (7)
M9	Right	42.9 ± 4 (8)	41.4 ± 2.7 (4)	46.4 ± 3.5 (3)	42.3 ± 3.3 (17)	40.1 ± 2.7 (5)	44.2 ± 2.4 (10)
	Left	41.9 ± 2.6 (5)	43.0/44.0 (2)	40.2/44.1 (2)	42.1 ± 2.4 (17)	40.1 ± 2.3 (4)	43.3 ± 2.1 (10)
M10	Right	48.5 ± 3.2 (8)	47 ± 2.2 (3)	50.9 ± 1.7 (4)	45.9 ± 3.9 (13)	42.7 ± 2.5 (4)	48.4 ± 2.8 (7)
	Left	48.3 ± 1.7 (7)	46.0/48.0 (2)	48.5 ± 1.7 (4)	45.8 ± 2.6 (16)	43.5 ± 1.5 (4)	47.1 ± 2.3 (9)
M12a	Right	44.7 ± 2.4 (7)	41.2/45 (2)	46 ± 1.9 (4)	43.3 ± 2.8 (11)	42.1 ± 2.9 (4)	44.3 ± 3.8 (4)
	Left	43.7 ± 7.2 (10)	40.8 (1)	46.5 ± 2.2 (7)	42.8 ± 2.9 (13)	35.5/42.3 (2)	43.5 ± 2.5 (8)
Retroversion	Right	35.2 ± 6.5 (6)	41.0 (1)	32.3 ± 6.1 (4)	34.0 ± 12.1 (10)	35.0/54.0 (2)	29.0 ± 10.8 (6)
angle	Left	30.8 ± 8.4 (10)	28.0/38.0 (2)	29.8 ± 9.6 (6)	24.6 ± 5.6 (11)	27.0 ± 7.2 (3)	23.3 ± 5.3 (7)
M5/M6	Right	1.25 ± 0.05 (13)	1.23 ± 0.06 (5)	1.26 ± 0.05 (7)	1.32 ± 0.09 (25)	1.30 ± 0.08 (8)	1.33 ± 0.10 (13)
	Left	1.22 ± 0.07 (16)	1.24 ± 0.08 (4)	1.22 ± 0.08 (10)	1.31 ± 0.12 (22)	1.29 ± 0.16 (8)	1.31 ± 0.12 (11)
Imax / Imin	Right	1.57 ± 0.19 (19)	1.56 ± 0.16 (7)	1.57 ± 0.23 (11)	1.68 ± 0.20 (23)	1.57 ± 0.21 (8)	1.73 ± 0.18 (14)
50%	Left	1.52 ± 0.21 (23)	1.55 ± 0.23 (8)	1.50 ± 0.21 (14)	1.67 ± 0.22 (23)	1.61 ± 0.28 (7)	1.69 ± 0.18 (13)
Robusticity	Right	18.9 ± 0.8 (11)	18.7 ± 0.4 (4)	18.9 ± 1.0 (6)	20.3 ± 1.3 (19)	20.2 ± 2.0 (5)	20.5 ± 0.5 (11)
index	Left	18.0 ± 1.2 (12)	18.5 ± 1.6 (4)	17.5 ± 0.7 (6)	19.3 ± 1.5 (17)	19.1 ± 1.2 (6)	19.3 ± 1.9 (9)
Standardised	Right	583.6 ± 187.7 (15)	479.2 ± 122.7 (3)	608.8 ± 205.5 (11)	839.3 ± 293.4 (21)	773.2 ± 345 (4)	870.5 ± 267.3 (14)
J 35%	Left	400.4 ± 133.1 (18)	474 ± 115.6 (4)	386.5 ± 136.6 (13)	682.3 ± 269 (22)	798.3 ± 236.3 (5)	642.4 ± 303.9 (14)
Standardised	Right	591.9 ± 188.4 (19)	580 ± 96.3 (7)	575.2 ± 225.4 (11)	1052.2 ± 307.5 (24)	943.3 ± 289.1 (6)	1063.5 ± 321 (16)
J 50%	Left	482.1 ± 152.2 (25)	548.9 ± 116.6 (8)	425 ± 133.3 (15)	790.4 ± 266.7 (23)	780.7 ± 170.7 (5)	793.1 ± 320.7 (15)

Table 3 Estimated stature for L3-088 and comparative samples / *Stature estimée pour L3-088 et les échantillons de comparaison*

	Estimated stature
Humerus L3-088 (Eq. Male humerus)	170.6 ± 4.4
Humerus L3-088 (Eq. Female humerus)	165.2 ± 4.3
MUP Males	173.0 ± 4.6 (13)
MUP Females	163.1 ± 4.7 (6)
LUP Males	162.4 ± 4.7 (17)
LUP Females	153.9 ± 4.3 (7)

perimeter (M7)/maximum length (M1) × 100)] of 18.6 lies in the middle of the range of variation seen for MUP male and female samples and below the values seen for the LUP (Table 2). This can also be illustrated by plotting the polar moment of area (*J*) at mid-distal diaphysis versus articular lengths (Fig. 4). Cussac L3-088 has a low value for J compared to its length and comes closer to the pattern of MUP than LUP individuals (Table 2).

The distal joints and entheses display no clear pathological changes. The surface of the medial epicondyle is heavily eroded but appears very bumpy. The medial epicondyle is well developed and very posteriorly projected. The radial fossa is nearly absent, whereas the coronoid fossa is well marked. The olecranon fossa is ovoid, large and shallow. The septal aperture is absent, but there is a marked depression at the bottom of the fossa (about 6 mm in diameter and ca. 3 mm in depth), the upper edge of this depression corresponding to the upper angle of the olecranon fossa (Fig. 5).

Discussion and Conclusions

This article presents the biological data for an isolated Late Pleistocene left humerus from the Cussac Cave, obtained through classical observations and imaging techniques. This complete bone is characterised by significant humeral retroversion, one of the largest seen in the Upper Palaeolithic sample. A large retroversion is mostly seen in MUP individuals, and the majority of paired humeri show a larger retroversion on the right side. It is thus surprising to find such a wide retroversion angle for the left side. This humerus also displays relatively marked lateral convexity of the shaft, marked intracortical porosity at three muscle attachment sites, moderate robusticity, a very posteriorly displaced and elongated medial epicondyle and a depression in the olecranon fossa.

There is strong evidence from sports medicine studies that regular forceful throwing results in more retroversion of the humerus of the throwing limb. Throwing athletes typically have wider retroversion angles in their throwing arm compared to their non-dominant arm and the arms of non-throwing controls [e.g. 30–32]. Based on these studies, a high degree of humeral retroversion, associated with significant bilateral asymmetry, has been linked to habitual throwing in prehistoric hunter-gatherer samples [19].

Intracortical porosity has recently been studied in detail in animal models and living human populations, especially in the relation to osteoporosis. It is quite clear that intracortical porosity increases with age [33,34], although differently between men and women, but apparently contradictory results have been obtained regarding the effect of activity. On the one hand, it has been shown for the femur that intracortical porosity in older individuals tends to be more frequent where bending stresses are low [34], and that porosity diminishes in growing bone in response to exercise [35]. On the other hand, high localised intracortical porosity has been observed in the exercised forearm of rats [36], and it has been shown directly or indirectly that porosity is greater (although to a lesser degree than in old individuals) in athletes compared to non-athletes [37,38]. The relationship between exercise and local intracortical porosity is unclear. It has been hypothesised that porosity enables an increased nutrient supply, eventually leading to periosteal apposition [37], reflecting a response to the generation of microdamage [38] or reducing the area available for the propagation of microcracks [39]. As data are lacking on cortical porosity distribution in the whole shaft of the humerus of living humans, we did not attempt to quantify the intracortical porosity of Cussac L3-088 for comparison. Given the localised pattern (i.e. in the area of muscle attachment sites) and the lack of macroscopic or microscopic signs of advanced age, it seems unlikely that the porosity seen in this humerus was associated with age-related bone loss, and is more likely to be linked to localised mechanical stimuli.It has been shown that a posteriorly oriented epicondyle “causes a displacement of maximum rotational efficiency towards a more pronated position of the forearm, leading to a gain of efficiency in the entire pronation range” [40, p. 217], and that an enlarged medial epicondyle increases this efficiency [41]. Moreover, these authors suggest that the orientation and morphology of the medial epicondyle can be modified, to some degree, during ontogeny in order to adapt to mechanical loadings [40,41].

The modification seen in the olecranon fossa of Cussac L3-088 evokes a space-occupying lesion. A virtually identical change has been observed previously in the left humerus of the Gravettian individual Baousso da Torre 1 [5]. Among the possible causes, an osteoid osteoma seems the most likely considering the very regular margin of this depression. Juxta- and intra-articular osteoid osteomas are rare, but can occur in the olecranon fossa, the nidus located subchondrally creating a crater-like imprint at the bottom of the fossa [42].

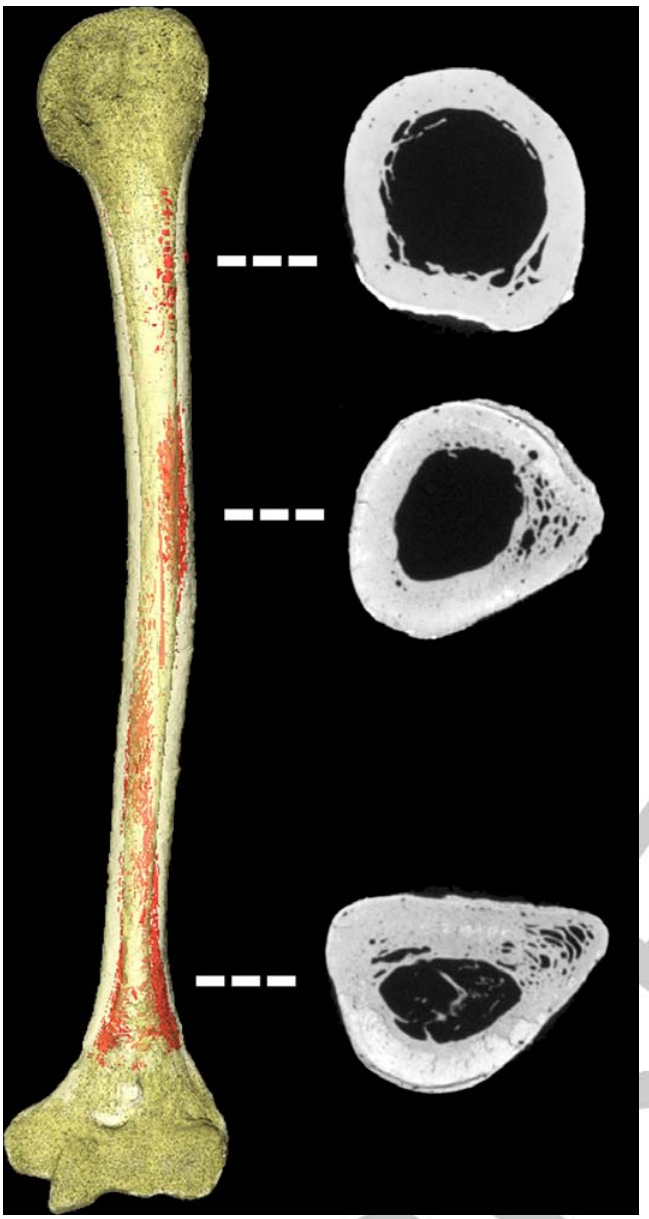

Fig. 3 Distribution of humeral intracortical porosity. 3D model of the humerus with regions of intracortical porosity indicated in red (left) and three transverse slices from different positions in the diaphysis, as indicated by the dashed white lines (right) / *Distribution de la porosité intracorticale. Modèle 3D de l'humérus avec les régions de porosité indiquée en rouge (à gauche) et trois coupes transverse dans la diaphyse (à droite), aux localisations indiquées par les lignes blanches pointillées*

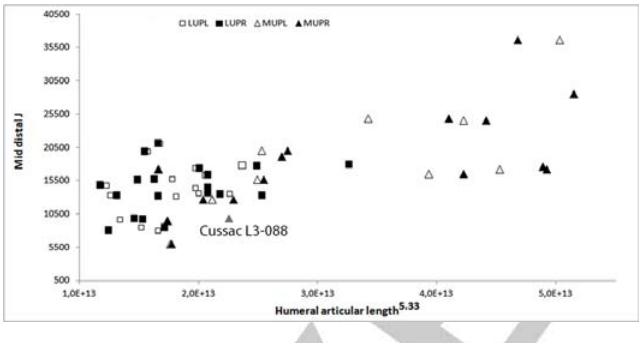

Fig. 4 Mid-distal polar moment of area (J) versus humeral articular length$^{5.33}$. LUPL: Left, Late-Upper Palaeolithic humeri; LUPR: Right, Late-Upper Palaeolithic humeri; MUPL: Left, Mid-Upper Palaeolithic humeri; MUPR: Right, Mid-Upper Palaeolithic humeri / *Moment d'inertie polaire (J) en mi-distal par rapport à la longueur articulaire de l'humérus$^{5.33}$. LUPL : humérus gauches du Paléolithique supérieur final ; LUPR : humérus droits du Paléolithique supérieur final ; MUPL : humérus gauches du Paléolithique supérieur moyen ; MUPR : humérus droits du Paléolithique supérieur moyen*

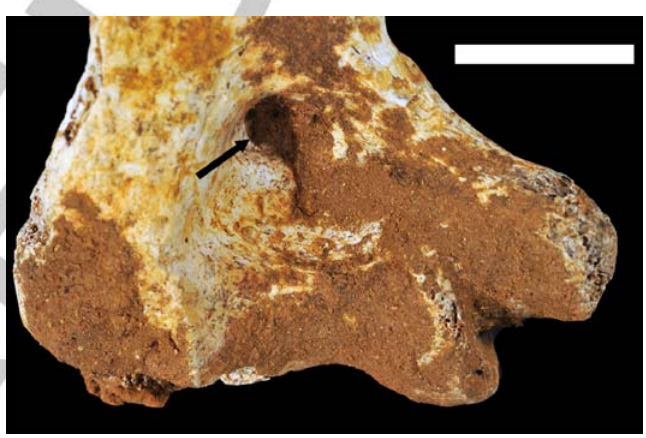

Fig. 5 Magnified view of the distal humerus. Marked depression at the bottom of the olecranon fossa indicated with a black arrow (scale = 2 cm) / *Vue rapprochée de la partie distale de l'humérus. La dépression marquée au fond de la fosse olécranienne est indiquée par la flèche noire (échelle = 2 cm)*

A less convincing cause may be a posteromedial olecranon impingement, which is a common injury encountered in the throwing elbow, and is commonly associated with osteoarthritic changes including the possible presence of loose bodies and chronic stress fracture at the olecranon process [43,44]. However, there is no sign of any abnormal contact of the medial olecranon with the medial wall of the olecranon fossa in Cussac L3-088.

The overhead throwing motion is mainly known from baseball pitchers. The pitching motion proceeds in six phases: wind-up, early cocking/stride, late cocking, acceleration, deceleration, and follow-through, the most stressful event arising in the late cocking phase which involves a very quick shift from extension–supination to flexion–pronation [45–47]. Many muscles are involved in the throwing motion, including the *m. deltoïdus* (mainly in the acceleration and deceleration phases), the *m. brachioradialis* (early

cocking, late cocking and deceleration phases) and the *m. triceps brachii* (mostly during the acceleration phase) [47,48].

Overall, it would be tempting to associate the very marked retroversion, the peculiar morphology and orientation of the medial epicondyle, and possibly the intracortical porosity and the change seen in the olecranon fossa, to mechanical stimuli related to the throwing motion. However, counterarguments need to be mentioned: the very rounded diaphysis at mid-shaft does not suggest specific bending constraints, the bone is not especially robust and individuals with left-dominated asymmetry are uncommon in the Upper Palaeolithic [49]. Moreover, a recent study indicates that while the contribution of the legs, torso and dominant shoulder to a spear throw are comparable in magnitude to that for a ball throw, the contribution of the arm differs significantly [50]. This indicates that the throwing motion models inferred from biomedical studies should be used with caution in discussions on past activities. Finally, due to the fact that we are dealing with an isolated bone, many factors cannot be controlled (e.g. age-at-death, sex, body mass, degree of asymmetry), making this interpretation rather speculative.

It is clear, however, that our study of Cussac L3-088, indirectly dated to the Gravettian, once again illustrates that i) the morphologies of MUP and LUP groups are quite different (although Upper Palaeolithic individuals are still often considered as a homogeneous group to which fossils from other human groups can be compared [e.g. 51,52]), and ii) new discoveries tend to dramatically increase the known range of variation for these periods.

Acknowledgements The authors thank the Cussac *Programme Commun de Recherche* for their productive teamwork on this exceptional site. They are grateful to the institutions, curators and researchers who provided access to their facilities and granted permission to examine the palaeoanthropological material used in the comparative samples. They also thank Ronan Ledevin (PACEA) for his support and help during the micro-computed tomography acquisition and analysis. They are grateful to the two anonymous reviewers and the editor-in-chief for their useful comments. This study was supported by the *Agence Nationale de la Recherche* (ANR) GRAVETT'OS (grant number ANR-15-CE-0004) and conducted in part with the help of the LaScArBx ANR-10-LABX-52.

Conflict of Interest: to come.

References

1. Trinkaus E (2000) Late Pleistocene and Holocene human remains from Paviland Cave. In: Aldhous-Green S (ed) Paviland Cave and the "Red Lady": a definitive report. Western Academic & Specialist Press Limited, Bristol, pp 141–99
2. Trinkaus E, Svoboda J (2006) Early modern human evolution in Central Europe. The people of Dolní Věstonice and Pavlov. Oxford University Press, New York, 489 p
3. Trinkaus E, Buzhilova AP, Mednikova MB, et al (2014) The people of Sunghir. Burials, bodies, and behavior in the earlier Upper Paleolithic. Oxford University Press, New York, 368 p
4. Villotte S, Chiotti L, Nespoulet R, et al (2015) Étude anthropologique des vestiges humains récemment découverts issus de la couche 2 de l'abri Pataud (Les Eyzies-de-Tayac-Sireuil, Dordogne, France). BMSAP 27:158–88
5. Villotte S, Samsel M, Sparacello V (2017) The paleobiology of two adult skeletons from Baousso da Torre (Bausu da Ture) (Liguria, Italy): implications for Gravettian lifestyle. C R Palevol 16:462–73
6. Guyomarc'h P, Samsel M, Courtaud P, et al (2017) New data on the paleobiology of the Gravettian individual L2A from Cussac cave (Dordogne, France) through a virtual approach. J Arch Sci Rep 14:365–73
7. Churchill SE, Formicola V, Holliday TW, et al (2000) The Upper Palaeolithic population of Europe in an evolutionary perspective. In: Roebroeks W, Mussi M, Svoboda J, Fennema K (eds) Hunters of the golden age. University of Leiden, Leiden, pp 31–57
8. Formicola V (2007) From the Sunghir children to the Romito dwarf: aspects of the Upper Paleolithic funerary landscape. Curr Anthropol 48:446–53
9. Henry-Gambier D (2008) Comportement des populations d'Europe au Gravettien : Pratiques funéraires et interprétations. Paleo 20:399–438
10. Holt BM, Formicola V (2008) Hunters of the Ice Age: the biology of Upper Paleolithic people. Am J Phys Anthropol 137:70–99
11. Villotte S, Churchill SE, Dutour O, et al (2010) Subsistence activities and the sexual division of labor in the European Upper Paleolithic and Mesolithic: evidence from upper limb enthesopathies. J Hum Evol 59:35–43
12. Aujoulat N, Geneste JM, Archambeau C, et al (2001) La grotte ornée de Cussac (Dordogne). Observations liminaires. Paleo 13:9–18
13. Jaubert J, Genty D, Valladas H, et al (2017) The chronology of human and animal presence in the decorated and sepulchral cave of Cussac (France). Quat Int 432:5–24
14. Henry-Gambier D, Courtaud P, Duday H, et al (2013) Grotte de Cussac (Le Buisson-de-Cadouin, Dordogne) : un exemple de comportement original pour le Gravettien. In: Jaubert J, Fourment N, Depaepe P (eds) Transitions, Ruptures et Continuité en Préhistoire : XXVII^{e} Congrès Préhistorique de France, Bordeaux - Les Eyzies 31 mai–5 juin 2010. Vol. 1. Société préhistorique française, Paris, pp 169–82
15. Villotte S, Santos F, Courtaud P (2015) In situ study of the Gravettian individual from Cussac cave, locus 2 (Dordogne, France). Am J Phys Anthropol 158:759–68
16. Peignaux C, Kacki S, Guyomarc'h P, et al (2019) New anthropological data from Cussac Cave (Gravettian, Dordogne, France): in situ and virtual analyses of Locus 3. C R Palevol 18:455–64
17. Bräuer G (1988) Osteometrie. In: Knussmann R (ed) Anthropologie: handbuch der vergleichenden Biologie des Menschen. G. Fischer, Stuttgart, pp 160–232
18. Hambucken A (1993) Variabilité morphologique et métrique de l'humérus, du radius et de l'ulna des Néandertaliens. Comparaison avec l'Homme moderne. Thèse d'Anthropologie. Université de Bordeaux-I, 316 p
19. Rhodes JA, Churchill SE (2009) Throwing in the Middle and Upper Paleolithic: inferences from an analysis of humeral retroversion. J Hum Evol 56:1–10

20. Sládek V, Trinkaus E, Hillson SW, et al (2000) The people of the Pavlovian. Skeletal catalogue and osteometrics of the Gravettian fossil hominids from Dolní Věstonice and Pavlov. Academy of Sciences of the Czech Republic, Brno, p 244
21. Dutailly B (2016) TIVMI, treatment and increased vision for medical imaging, 2.1 ed.AU: Please provide the complete reference.
22. Ruff CB (2002) Long bone articular and diaphyseal structure in Old World monkeys and apes. I: locomotor effects. Am J Phys Anthropol 119:305–42
23. Nagurka M, Hayes W (1980) An interactive graphics package for calculating cross-sectional properties of complex shapes. J Biomech 13:59–64
24. Rhodes JA (2006) Adaptations to humeral torsion in medieval Britain. Am J Phys Anthropol 130:160–6
25. Stahl Gretsch L-I (2005) Les squelettes « magdaléniens » de Veyrier remis en contexte. ASSPA 88:283–91
26. Ruff CB (2000) Biomechanical analyses of archaeological human skeletons. In: Katzenberg MA, Saunders SR (eds) Biological anthropology of the human skeleton. Wiley-Liss, New York, pp 71–102
27. Ruff CB, Trinkaus E, Walker A, et al (1993) Postcranial robusticity in Homo. I: Temporal trends and mechanical interpretation. Am J Phys Anthropol 91:21–53
28. Trotter M, Gleser GC (1952) Estimation of stature from long limb bones of American Whites and Negroes. Am J Phys Anthropol 10:463–514
29. Formicola V (2003) More is not always better: Trotter and Gleser's equations and stature estimates of Upper Paleolithic European samples. J Hum Evol 45:239–44
30. Chant CB, Litchfield R, Griffin S, et al (2007) Humeral head retroversion in competitive baseball players and its relationship to glenohumeral rotation range of motion. J Orthop Sports Phys Ther 37:514–20
31. Osbahr DC, Cannon DL, Speer KP (2002) Retroversion of the humerus in the throwing shoulder of college baseball pitchers. Am J Sports Med 30:347–53
32. Pieper HG (1998) Humeral torsion in the throwing arm of handball players. Am J Sports Med 26: 247–53
33. Bousson V, Meunier A, Bergot C, et al (2001) Distribution of intracortical porosity in human midfemoral cortex by age and gender. J Bone Miner Res 16:1308–17
34. Thomas CDL, Feik SA, Clement JG (2005) Regional variation of intracortical porosity in the midshaft of the human femur: age and sex differences. J Anat 206:115–25
35. Forwood MR, Burr DB (1993) Physical activity and bone mass: exercises in futility? Bone Miner 21:89–112
36. Warden SJ, Fuchs RK, Castillo AB, et al (2007) Exercise when young provides lifelong benefits to bone structure and strength. J Bone Miner Res 22:251–9
37. Ackerman KE, Putman M, Guereca G, et al (2012) Cortical microstructure and estimated bone strength in young amenorrheic athletes, eumenorrheic athletes and non-athletes. Bone 51:680–7
38. Feldman S, Capozza RF, Mortarino PA, et al (2012) Site and sex effects on tibia structure in distance runners and untrained people. Med Sci Sports Exerc 44:1580–8
39. Osterhoff G, Morgan EF, Shefelbine SJ, et al (2016) Bone mechanical properties and changes with osteoporosis. Injury 47: S11–S20
40. Ibáñez-Gimeno P, Galtés I, Jordana X, et al (2013) Entheseal changes and functional implications of the humeral medial epicondyle. Int J Osteoarchaeol 23:211–20
41. Ibáñez-Gimeno P, Galtés I, Jordana X, et al (2014) Biomechanics of forearm rotation: force and efficiency of pronator teres. PLoS One 9:e90319
42. Font Segura J, Barrera-Ochoa S, Gargallo-Margarit A, et al (2013) Osteoid osteoma of the distal humerus mimicking sequela of pediatric supracondylar fracture: arthroscopic resection — case report and a literature review. Case Rep Med 2013:6
43. Cain ELJ, Dugas JR, Wolf RS, et al (2003) Elbow injuries in throwing athletes: a current concepts review. Am J Sports Med 31:621–35
44. Ko CC, Tai MH, Lin CH, et al (2016) Posteromedial olecranon impingement of the pitching elbow: additional findings provided by CT. Eur J Radiol 85:211–17
45. Bramhall JP, Scarpinato DF, Andrews JR (1994) Injuries in throwing sports. In: Renström P (ed) Clinical practice of sports injury prevention and care (the encyclopaedia of sport medicine, volume 5). Blackwell Scientific Publications, Oxford, pp 446–9
46. Coudreuse JM, Parier J (2003) Pathologies du lancer : l'épaule et le coude. Médecins du Sport 13:15–27 Merci de vérifier la référence
47. Seroyer ST, Nho SJ, Bach BR, et al (2010) The kinetic Chain in overhand pitching: its potential role for performance enhancement and injury prevention. Sports Health 2:135–46
48. DiGiovine NM, Jobe FW, Pink M, et al (1992) An electromyographic analysis of the upper extremity in pitching. J Shoulder Elbow Surg 1:15–25
49. Sparacello VS, Villotte S, Shackelford LL, et al (2017) Patterns of humeral asymmetry among Late Pleistocene humans. Com R Palevol 16:680–9
50. Maki JM (2013) The biomechanics of spear throwing: an analysis of the effects of anatomical variation on throwing performance, with implications for the fossil record. PhD thesis. Washington University, St. Louis, p 287
51. Pomeroy E, Mirazón Lahr M, Crivellaro F, et al (2017) Newly discovered Neanderthal remains from Shanidar Cave, Iraqi Kurdistan, and their attribution to Shanidar 5. J Hum Evol 111:102–18
52. Stoessel A, David R, Gunz P, et al (2016) Morphology and function of Neandertal and modern human ear ossicles. Proc Natl Acad Sci USA 113:11489–94